AD-A156 999 ANALYSIS OF A GAS GENERATOR SYSTEM(U) ARMY BALLISTIC RESEARCH LAB ABERDEEN PROVING GROUND MD C W NELSON ET AL. APR 85 BRL-TR-2648 1/1

UNCLASSIFIED F/G 13/7 NL

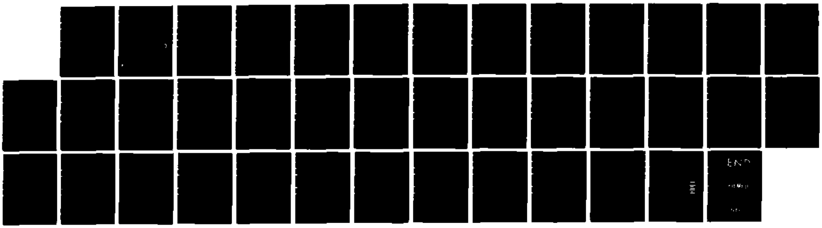

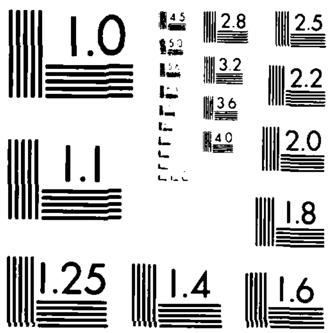

MICROCOPY RESOLUTION TEST CHART

AD-A156 999

2

AD

US ARMY
MATERIEL
COMMAND

TECHNICAL REPORT BRL-TR-2648

ANALYSIS OF A GAS GENERATOR SYSTEM

Carl W. Nelson
Douglas E. Kooker

April 1985

APPROVED FOR PUBLIC RELEASE; DISTRIBUTION UNLIMITED.

US ARMY BALLISTIC RESEARCH LABORATORY
ABERDEEN PROVING GROUND, MARYLAND

85 7 1[illegible] 017

UNCLASSIFIED
SECURITY CLASSIFICATION OF THIS PAGE (When Data Entered)

REPORT DOCUMENTATION PAGE		READ INSTRUCTIONS BEFORE COMPLETING FORM
1. REPORT NUMBER Technical Report BRL-TR-2648	2. GOVT ACCESSION NO. AD-A156999	3. RECIPIENT'S CATALOG NUMBER
4. TITLE (and Subtitle) Analysis of a Gas Generator System		5. TYPE OF REPORT & PERIOD COVERED Final
		6. PERFORMING ORG. REPORT NUMBER
7. AUTHOR(s) Carl W. Nelson and Douglas E. Kooker		8. CONTRACT OR GRANT NUMBER(s)
9. PERFORMING ORGANIZATION NAME AND ADDRESS US Army Ballistic Research Laboratory ATTN: AMXBR-IBD Aberdeen Proving Ground, MD 21005-5066		10. PROGRAM ELEMENT, PROJECT, TASK AREA & WORK UNIT NUMBERS 1L161102AH43
11. CONTROLLING OFFICE NAME AND ADDRESS US Army Ballistic Research Laboratory ATTN: AMXBR-OD-ST Aberdeen Proving Ground, MD 21005-5066		12. REPORT DATE April 1985
		13. NUMBER OF PAGES 36
14. MONITORING AGENCY NAME & ADDRESS(if different from Controlling Office)		15. SECURITY CLASS. (of this report) UNCLASSIFIED
		15a. DECLASSIFICATION DOWNGRADING SCHEDULE

16. DISTRIBUTION STATEMENT (of this Report)

Approved for Public Release; Distribution Unlimited.

17. DISTRIBUTION STATEMENT (of the abstract entered in Block 20, if different from Report)

18. SUPPLEMENTARY NOTES

19. KEY WORDS (Continue on reverse side if necessary and identify by block number)

Gas Generator
Heat Transfer
Burning-Rate
Math Models
Combustion
Combustion Thermodynamics
Fluid Mechanics

20. ABSTRACT (Continue on reverse side if necessary and identify by block number)

A small gas generator suddenly failed in acceptance tests after a string of successes. Intensive tests and rough calculations said that heat transfer to the cold surroundings, coupled with a change in burning-rate exponent at low pressure, caused the failure. Two math models, a lumped parameter model and a full one-dimensional fluid mechanics model were devised to explain the interaction among combustion, heat transfer, and fluid mechanics.

DD FORM 1 JAN 73 1473 EDITION OF 1 NOV 65 IS OBSOLETE

UNCLASSIFIED
SECURITY CLASSIFICATION OF THIS PAGE (When Data Entered)

20. Abstract (Cont'd):

The models predict that a reasonable estimate of heat loss does not, by itself, explain the failures. The success of an isolation venturi can only be partially explained by heat transfer. Suspicion then rests on the assumption of equilibrium combustion thermodynamics at the very cold temperatures where the failures occurred. Variations with age and propellant batch are still not exonerated, even though the critical problem seems to have been solved.

TABLE OF CONTENTS

LIST OF FIGURES

I. INTRODUCTION

September started badly. A string of 14 successful tests of a gas generator at its cold-temperature limit ended in the simultaneous failure of two units. The meager data suggested four plausible causes: moisture intrusion, gas leak, depressurization extinguishment, or marginal design. A diagnostic test program was designed to isolate the most likely cause among moisture, leaks, and ignition overdrive. Elliott at the Jet Propulsion Laboratory started building a mathematical model of the generator.

October ended badly. Only one test condition (moisture) duplicated the failure. But all tests with the entire generator soaked at the cold-temperature limit failed by dropping below the minimum acceptable pressure. Although moisture probably caused the specific September failures, a fatal design flaw had been exposed. Tests discredited the prime suspect, leakage. If it wasn't moisture or leaks, what was it?

The clearest clue came from Elliott's model where the low pressure could be explained by a steeper than expected dependence of propellant burning rate on pressure at low pressure. But there were essentially no useful data on cold-temperature burning rate at that low pressure. If the slope were high, any drop in pressure would tend to continue. Thus when the cold hardware cooled the gases, the pressure drop from its ignition peak would not stop at the design limits calculated with the slope obtained from higher pressure burning-rate data.

Two changes were considered: a new design or a higher cold temperature limit. Schedule demands said raise the limit, which had been -25 F, to where the problem disappeared. *No one knew that* limit yet. But when a conservative limit of 20 F also failed, design change awakened. The easiest change added a venturi to isolate the combustion chamber from pressure loss in the downstream tubing. Meanwhile, the propellant lot that had been used for two years had run out and newly made propellant was being delivered. The combination of the venturi and new propellant ended the failures.

The hardware now worked even at the lowest temperature but it was not yet clear why. Would it still work two years later? What were the variation limits of combustion? Burning-rate tests validated the slope-break hypothesis and found some lot-to-lot variation in the low-pressure slope and the break point.

Three circumstances created the mystery: (1) inadequate knowledge of the low-pressure burning rate, (2) no useful simulation of the generator operation, and (3) inadequate recognition of the coupling among heat transfer, pressure, and burning rate. What remained was to explain the success, the failure, and the probability of repeating the failure.

II. THE GENERATOR DESIGN

The generator burns an ammonium-nitrate-oxidized rubber propellant in an end-burning grain to produce a clean, cool (1300 K) gas. The gas passes through a coarse pre-filter, a swirl flow centrifugal filter, a massive valve, and 40 cm of metal tubing to exit a deLaval nozzle. In the ignition sequence,

a squib-activated igniter spews hot gas and particles onto a pellet of an ammonium-perchlorate-based propellant (denoted as Ignition Pellet) which, in turn, furnishes enough hot gas to ignite the main propellant grain and a booster pellet of the same composition. After about one centimeter of burning of the main grain, the propellant geometry becomes a constant-area end-burning grain. All tubing is large enough to keep the flow velocity below 20 m/s.

A venturi of throat area slightly larger than the nozzle was inserted just upstream of the valve and the last 30 cm of tubing.

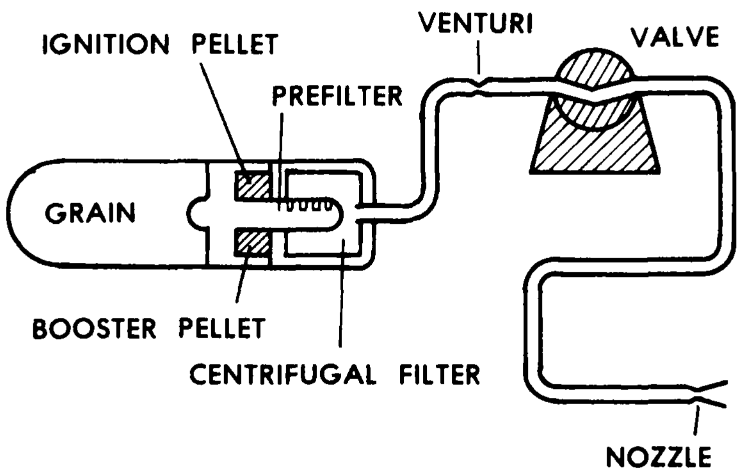

Figure 1. Schematic of Generator

III. MODELING APPROACH

Two models were developed in this study: a one-dimensional-flow model and a lumped-parameter model. The lumped-parameter model divides the generator into two chambers separated by the venturi. It ignores axial variation of the flow except as the downstream chamber is separate from the upstream chamber. The one-dimensional-flow approach addressses the axial dependence of the fluid mechanics from propellant surface to the exit nozzle. The one-dimensional model is more accurate, but expensive. The crude but thrifty lumped-parameter model allows many arbitrary changes of input data or equations for sensitivity tests. In retrospect the two model approach proved wise.

IV. A LUMPED-PARAMETER MODEL

The generator will be treated as two chambers separated by a venturi. The upstream chamber (denoted 1) includes the propellant combustion chamber, the filters, and the tubing up to the venturi. The downstream chamber (denoted 2) includes the valve, and the downstream tubing to the nozzle. Ordinary differential equations describe conservation of mass and energy in each chamber.

$$\frac{d}{dt}(\rho V)_1 = \omega_{prop} - \omega_{ven} \tag{1}$$

$$\frac{d}{dt}(\rho V)_2 = \omega_{ven} - \omega_{noz} \tag{2}$$

$$\frac{d}{dt}(\rho V c_v T)_1 = \omega_{prop}\, c_p T_{prop} - \omega_{ven} c_p T_1 - q_1 \tag{3}$$

$$\frac{d}{dt}(\rho V c_v T)_2 = \omega_{ven} c_p T_1 - \omega_{noz} c_p T_2 - q_2 \tag{4}$$

where ω_{prop}, ω_{ven}, and ω_{noz} are mass fluxes from the propellant, through the venturi, and nozzle, respectively. The term q is heat loss from the volume in question.

Heat transfer from the gas to its bounding surfaces is by convection,

$$q_w = h_c\,(T_g - T_w) \tag{5}$$

where the coefficient, h_c, depends on gas properties and velocity. Heat loss to the surroundings is by unsteady convection to the combustion-chamber head, the phenolic filter, and the valve. It is by free convection and radiation from the tube walls.

The internal convective coefficient was taken from a design analysis where it depended only on mass flow rate, once all other conditions were fixed. Wide variance in flow velocity from the reference condition would introduce additional error.

$$h_c = 110\left(\frac{m}{.003}\right)^{0.8} \quad [\mathrm{BTU/(hr\text{-}ft^2\text{-}sec)}] \tag{6}$$

where m is mass flow rate in lbm/sec. Unsteady conduction may be approximated by Goodman's cubic profile to yield surface temperature,[1]

$$T_w = T_o - n + [(T_o - n)^2 + 2nT_g - T_o^2]^{1/2} \tag{7}$$

where $n \equiv \frac{2}{3} h_c\, H/k^2$,

[1] T.R. Goodman, "Application of Integral Methods to Transient Nonlinear Heat Transfer," Advances in Heat Transfer, Ed. By T.F. Irvine and J.P. Hartnett, Vol. 1, Academic Press, 1964.

$$H = \int_o^t \alpha h_c (T_g - T_w) dt \ , \quad (8)$$

and α is thermal diffusivity. Radiation is by the standard,

$$q_r = \sigma \ (T_w^4 - T_o^4) \quad (9)$$

where the temperature of the surroundings, T_o, is the initial temperature.

Burning rate of the propellant comes from the propellant-maker's test data. The rate is fitted to the usual power-law dependence on pressure,

$$r = aP^n \quad . \quad (10)$$

This generator had a peculiarity in that the burning rate of the main-grain propellant had a much higher exponent (n) at low pressure than at high pressure (see Table 1). No problem is introduced to the modeling once the data are available and correctly interpreted.

Flow through the nozzle is assumed choked, quasi-steady, and isentropic and thus calculated by

$$\omega_{noz} = A_{t_n} \ P_2 \ [\frac{\gamma}{RT_2}]^{1/2} \ (\frac{2}{\gamma+1})^{\frac{\gamma+1}{2(\gamma-1)}} \quad (11)$$

where P_1 and P_2 are pressures in the upstream and downstream chambers, respectively. A_{t_n} is the cross-sectional area of the nozzle throat. The gas temperature (T_2) used here was not the average chamber temperature. Instead, the axial temperature drop through the downstream chamber was estimated, and a nozzle inlet temperature calculated. The result is a lower temperature and higher mass flow rate than would be calculated by a purely lumped-parameter approach.

Mass input to the upstream chamber from propellant combustion is

$$\omega_{prop} = r\rho_s S \quad . \quad (12)$$

Flow through the venturi from upstream to downstream chamber depends on whether the venturi is choked. The criterion for choking comes from isentropic flow. The venturi is choked (and obeys an equation similar to Eq. (11)) whenever

$$P_2 < P_1 \ [1 + (\frac{\gamma-1}{2}) \ M^2]^{(\frac{\gamma}{1-\gamma})} \quad (13)$$

where M satisfies

$$\frac{A_{t_v}}{A_2} = G_f M \left[1 + \frac{\gamma-1}{2} M^2\right]^{-\frac{\gamma+1}{2(\gamma-1)}} , \tag{14}$$

G_f is defined in Eq. (28), and A_2 is the cross-sectional area of the tubing just downstream of the venturi. In principle, it is unchoked under any other condition. In practice, the numerics behave badly when the flow depends on both upstream and downstream pressure. Smooth calculations must either restrict the time step or revamp the integration. The model chooses between two venturi flow conditions, fully choked or no flow. The effect should be small in the upstream chamber which is the target of this analysis. For designs with no venturi or a small area ratio from tube to venturi, the model is inadequate.

Burning surface comes from geometric calculations of the generator designers. The surface is essentially constant after 3 cm burned and no longer dominates pressure changes. Expected variations in area after the 3 cm should affect the steady pressure level only by a factor of a few percent. A coning effect may increase the area by five percent which translates to a 10% pressure increase IF the burning rate were the same on all parts of the exposed surface. Slower burning at the edges, due to heat loss through the side wall, will cause the coning. The net result: a small effect on the steady pressure.

Ignition of the two pellets and the main grain need not be simultaneous. A reasonable starting condition is ignition of the hot pellet (AP propellant) and both chambers filled with that combustion product gas. Ignition of the AN propellant (booster pellet and main grain) can then be calculated from heat transfer to the surface and an ignition criterion. Heat transfer for ignition is by the same convection and unsteady conduction. The simplest ignition criterion is surface temperature. Since there seem to be no ignition data for the propellant, the ignition temperature is arbitrary. Temperatures below 800K assure ignition and do not violate widely-held theories. At higher temperatures ignition depends strongly on heat transfer competition. A high coefficient helps heat the propellant faster but also cools the gas faster. The race frequently goes to the cooling.

The heat transfer coefficient inside the combustion chamber is itself uncertain. Gas velocity is low near the grain and convective heat transfer is inefficient. But the grains ignite even when the generator fails later. The coefficient must then be high enough to assure ignition. A simpler approach would be immediate and simultaneous ignition of all surfaces. The debate is probably academic since test failures seem unconnected to ignition.

The uncertain heat transfer affects more than ignition. Heat transfer to the generator head and filters depends intimately on the coefficient. The centrifugal filter will have a higher gas velocity and thus a considerably higher coefficient than the gas in contact with the propellant surfaces. The phenolic filter has a low thermal conductivity and therefore heats rapidly at its surface, reducing the heat transfer quickly.

Data obtained from various sources for nominal conditions for the generator design are given in Table 1 (see page 14). Propellant burning rate measurements showed evidence of lot-to-lot variation. The data given here are for a 'new' lot.

V. ONE-DIMENSIONAL FLOW MODEL

The lumped-parameter model above is based on assumptions which trade accuracy for simplicity and economy. However, some questions about system behavior demand a more detailed analysis. Substantial heat loss to cold boundaries can lead to axial property variations throughout the system. The behavior of both the nozzle and the venturi will be sensitive to the local flow properties at their entrance planes. Since the system failure can apparently be reversed by addition of the venturi, it is important to explain how this device alters the flow field.

The flow field is assumed one-dimensional and unsteady. One-dimensional flow is a reasonable assumption everywhere except in the combustion chamber and separator chamber (centrifugal filter) which involve low speed three-dimensional flow. To avoid this complication, the flow in each chamber is modeled as a reservoir problem, i.e., the influx is assumed to stagnate in the chamber and the outflux is accelerated from the local stagnation condition. However, a further complication arises when the usual equations of motion are applied to the tubing, venturi, and nozzle. The fact that both the venturi and nozzle have large values of entrance area/throat area (33 for venturi, 67 for the nozzle) requires extremely small grid spacing within these devices to resolve the flow field, particularly if the operation may switch between unchoked and choked. Stability then forces a prohibitively small maximum time step, making the simulation impractical. A reasonable alternative is construction of special flow field elements which assume inviscid, quasi-steady flow. Note here that quasi-steady means the interior flow of the element responds instantaneously to changes at its boundaries; it does not mean steady-state flow. These elements are explained in greater detail below. Finally, combustion products from both kinds of solid propellant are treated as ideal gases. Mixture properties for the system flow field are adjusted (artificially) in proportion to the mass flow rate from each propellant, ignoring the propagation of these changes along streamlines.

A. Continuous Flow Field

The pipe or tubing flow field is described by the solution to the one-dimensional unsteady equations of motion (accounting for wall heat loss) given in conservative form by

mass

$$\rho_t + m_z = 0 \tag{15}$$

propellant. If there is an age effect, the margin provided by the venturi may not be enough. A slightly larger venturi (3%) with the old propellant failed. The safety margin cannot be estimated from the data and analysis to date. On the plus side, the propellant has long been used in other applications with no strong evidence of aging.

4. What causes the pressure difference between venturi and nozzle? Neither model calculates it. Nominal model input calculates unchoking of the venturi just after peak pressure with nearly equal pressures thereafter; but tests typically show a continuous difference of about 0.7 MPa.

VIII. QUANDARY

Is the probability of failure of the present design high enough to justify more investment in understanding? The models do not presently qualify as an engineering tool. Continued success in tests will make the problem seem moot. But the issue of age-related change will not be answered until two years pass and test results are then compared to early production results. If and when the first test failure appears, the models will be asked to steer the engineering of the repair. But only if the manifest inaccuracies are removed can their answers be trusted to be any better than the crude calculations on which the design already rests.

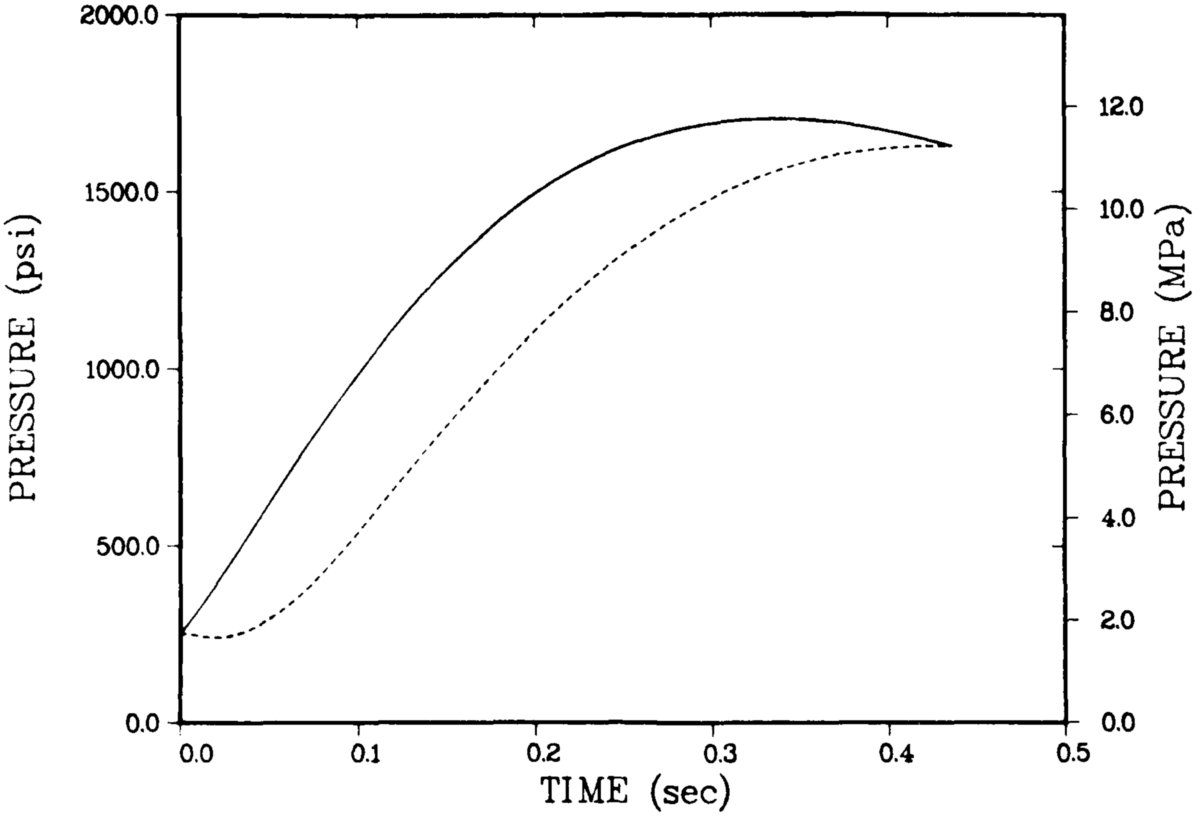

Figure 11. Pressure Time-History Predicted by One-Dimensional Model. Incomplete Combustion. Solid Line = Combustion Chamber, Dashed Line = Nozzle Entrance Plane.

VII. QUESTIONS STILL LURKING

1. How did heat transfer cause the failures? Its guilt was demonstrated in tests that succeeded when the valve and downstream tubing remained at the ambient California fall temperatures and only the parts upstream of the valve were conditioned to cold temperature. Simple sensible heat loss through an ideal equation of state for equilibrium combustion products does not explain it. Incomplete combustion may. The investigation ended without a useful post-mortem. Also unexplained was a gradual decline in pressure for about 25 seconds to the unacceptably low but steady pressure.

2. How did the venturi solve the problem? The basis for the predictions of the venturi's performance is attacked by the finding that only incomplete combustion recreates the measured pressure. Venturi design calculations were done with equilibrium composition assumptions.

3. Will the fix stay fixed? Propellant aging cannot be ruled out on the evidence. The transition from success to failure happened with two-year-old propellant. All the successful tests of the venturi occurred with new

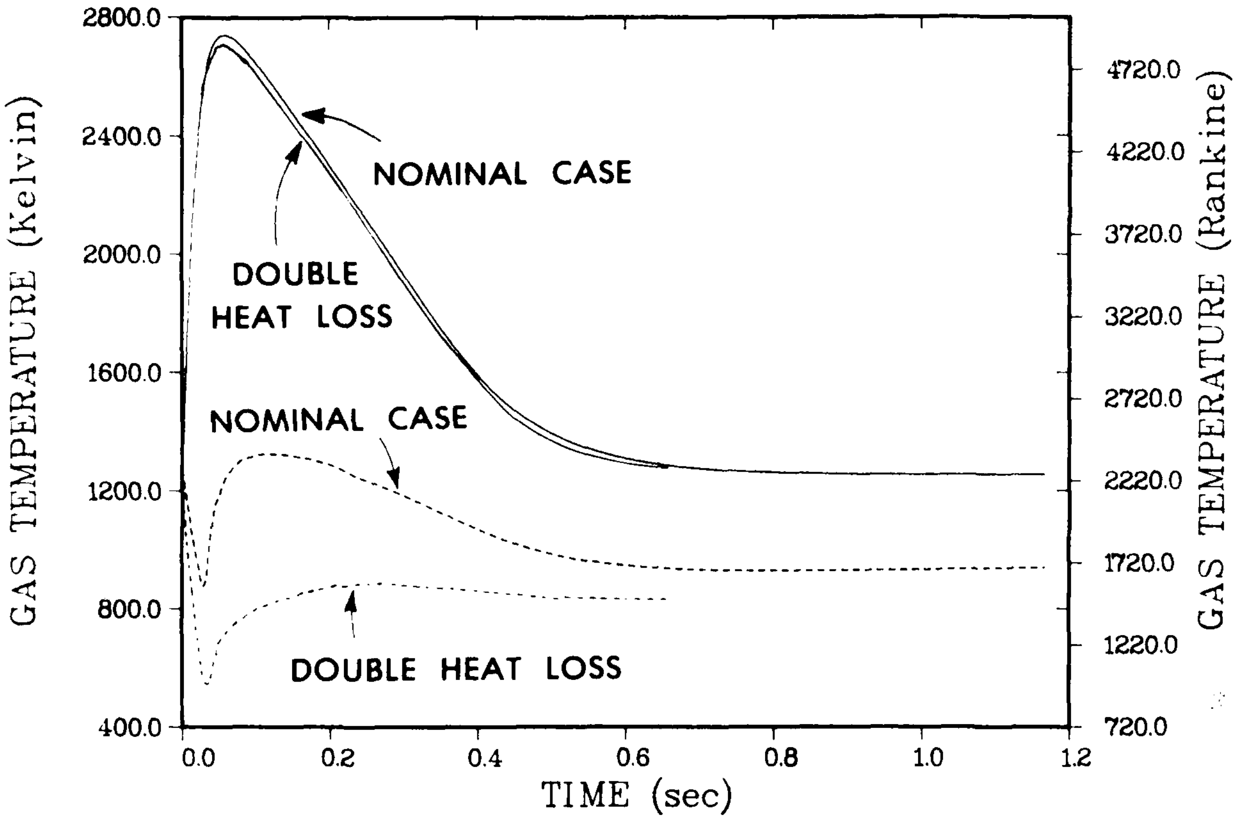

Figure 10. Temperature Time-History Predicted By One-Dimensional Model. Solid Line = Exit of Dual Chambers, Dashed Line = Nozzle Entrance Plane.

Because heat loss seems unable to explain the system behavior, attention focused on the possible lack of gas-phase thermodynamic equilibrium as suggested by trials with the lumped-parameter model. Setting the heat transfer coefficients at their nominal values and then imposing a fixed state of incomplete combustion ($\gamma-1$ = half value, $\mathcal{M}$ = three times nominal, T_f = 60% nominal) for both propellants produces the results shown in Figure 11 (also on Figure 9 to scale). These pressure time-history predictions are much closer to the experimental data, although the simulation again insists that the venturi will unchoke (at t ≈ 0.45 sec) after maximum chamber pressure is attained.

The dramatic improvement in the predictions strongly suggests that the gas-phase combustion products may be undergoing a complex "shifting" equilibrium, possibly with condensation. This could have an important influence on the presence of a shock wave in the venturi. The addition of this complicated chemistry to the flow field was beyond the scope of the present study.

system behavior is the same. It should be emphasized that doubling the heat loss to the valve and tubing which separates the venturi from the nozzle is not sufficient to keep the venturi choked.

Given the constraints of the model, the simulations demonstrate that only a shock wave downstream of the choked venturi is capable of creating the magnitude of total pressure loss measured in the actual gas generator.

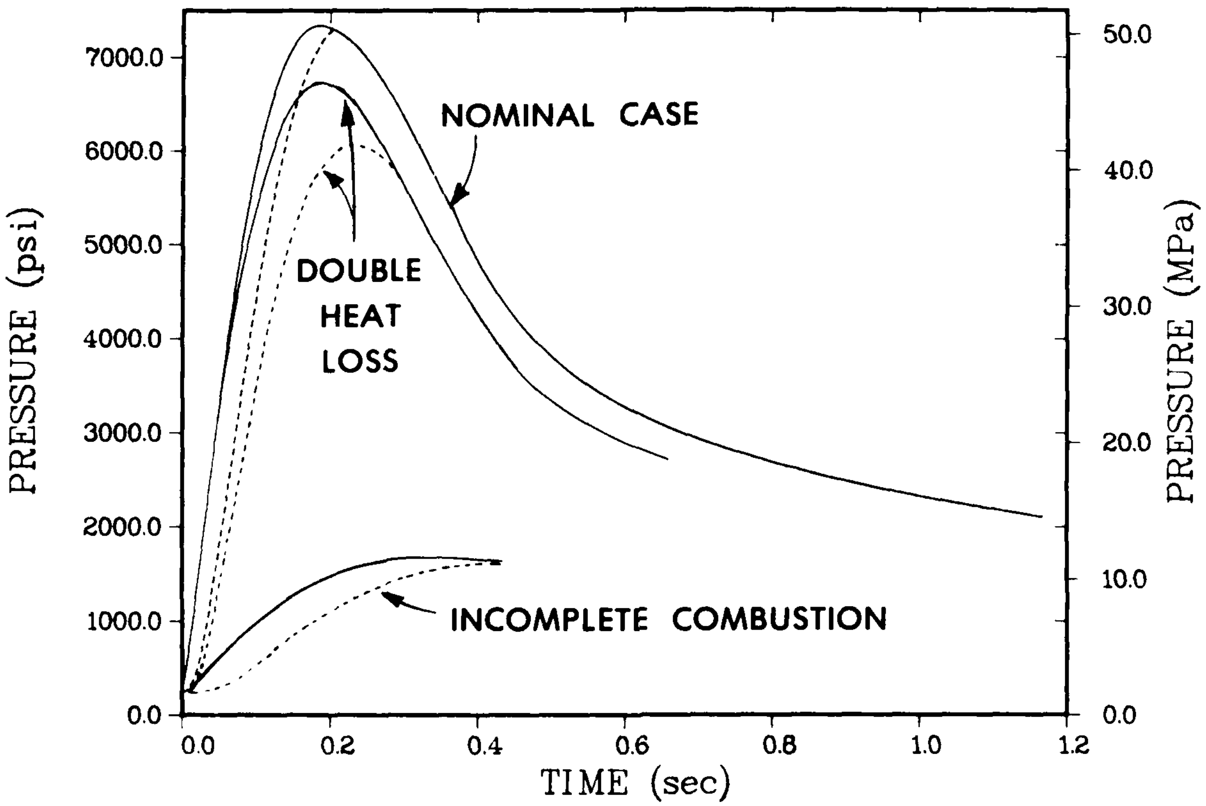

Figure 9. Pressure Time-History Predicted by One-Dimensional Model. Solid Line = Combustion Chamber, Dashed Line = Nozzle Entrance Plane.

However, fluid mechanics coupled with the assumption of gas-phase equilibrium thermochemistry predicts the venturi will not remain choked after maximum pressure has been achieved.

An objective for the modeling was to predict the influence of heat loss on the flow field temperatures. Figure 10 shows a comparison of temperature time-histories for the two cases discussed above. The solid lines represent gas temperature at the exit of the dual chambers, and the dashed lines denote gas temperature at the nozzle entrance plane. The difference between these two values measures the effect of heat loss. Note that in both cases, the temperatures become nearly time invariant after the order of 1 sec. Thus, thermal equilibrium with the surroundings is established much sooner than the time required for the system to "fail."

Flow equations seem an unlikely source of the pressure disagreement, and burning rate was well characterized by independent tests. Heat transfer offers the best first guess for the difference since it was suspected that heat transfer caused the problem in the first place. But reasonable variations in the heat transfer descriptions do not produce a credible change in the peak pressure without obliterating some other aspect of the problem. Enough heat transfer to reduce the pressure peak leads to gas temperatures well below the limits of equilibrium thermodynamics.

This led to the speculation that the gas thermodynamics vary from the expected equilibrium. Some incomplete combustion or subsequent condensation will significantly change the thermodynamic properties of the product gas. Arbitrary variations in thermodynamics could easily be made to test hypotheses about gas chemistry in numerical experiments. Full and defensible chemical effects are left for another day. Physical evidence for a non-equilibrium condition comes from window-bomb tests by the Jet Propulsion Laboratory (Leon Strand). Films of the combustion show hot ash, a less visible flame, and a larger ash residue at lower pressures.

For thermodynamic consistency, a mixture of gases was assumed to consist of fully reacted equilibrium products and an arbitrary intermediate product of incomplete combustion. The progress variable that controlled the conversion of intermediate to final products could also be arbitrary. Only simple linear time dependence was tried. Trial and error variations in $\gamma, \mathcal{M}$, T_f were made until calculated pressures matched test results. The values to produce this agreement were: $(\gamma-1.)$ half nominal value, $\mathcal{M}$ three times nominal, and T_f 60% of nominal. Time dependence of the progress variables ended arbitrarily at 2 sec.

Ignition of only part of the propellant surface is another candidate for error source. If the burn rate exponent (Eq. (10)) is 0.45, a pressure drop by a factor of three would need surface area of roughly half the geometric area. Given the highly gaseous igniter pellet products, a half ignited surface seems unlikely.

B. One-Dimensional Flow Model

Figure 9 shows a comparison of pressure time-histories predicted by the one-dimensional model for three different cases. The solid lines represent combustion chamber pressure, while the dashed lines denote static pressure at the entrance plane to the nozzle. Two important results are demonstrated by the predictions for the nominal case. First, maximum chamber pressure is greater than 7 Kpsi, in the range predicted by the lumped-parameter model. Second, the venturi unchokes soon after the combustion chamber achieves maximum pressure, e.g., approximately 0.2 sec in this case. (When the dashed and solid lines become coincident on the scale of the plot, the venturi is operating subsonic.) Both features are in direct conflict with the experimental data. Because of the uncertainty associated with some aspects of the heat transfer, the case was rerun after setting all heat transfer coefficients to twice their nominal values. These results (labeled Double Heat Loss) are shown in Figure 9 and confirm the conclusion from the lumped-parameter model that system behavior is relatively insensitive to changes in heat transfer. The venturi remains choked for a longer time, but the general

in the model results. Choking in the venturi is one possible explanation as is a pressure flow loss in the tubing. Unfortunately, neither explanation is supported by model findings or by fluid mechanics intuition.

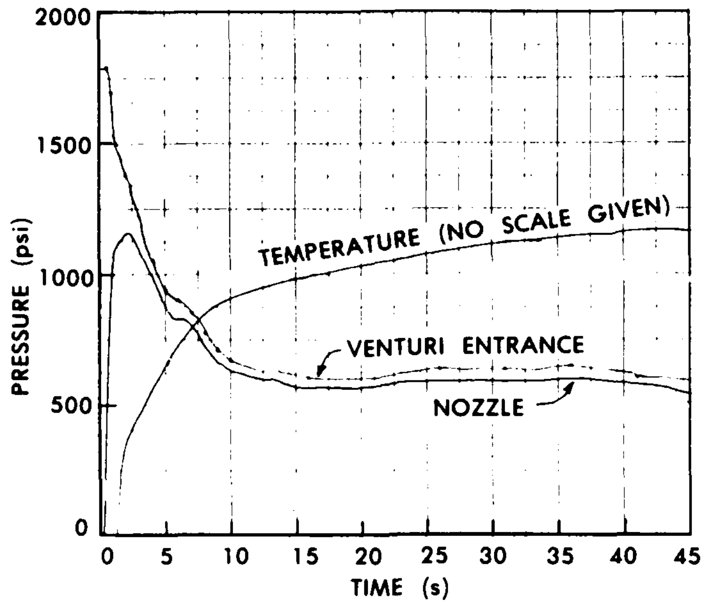

Figure 7. Typical Cold-Temperature Test Pressures

At long times the predicted and measured pressures agree. Figure 8 shows calculated pressures out to 65 seconds for the upstream chamber.

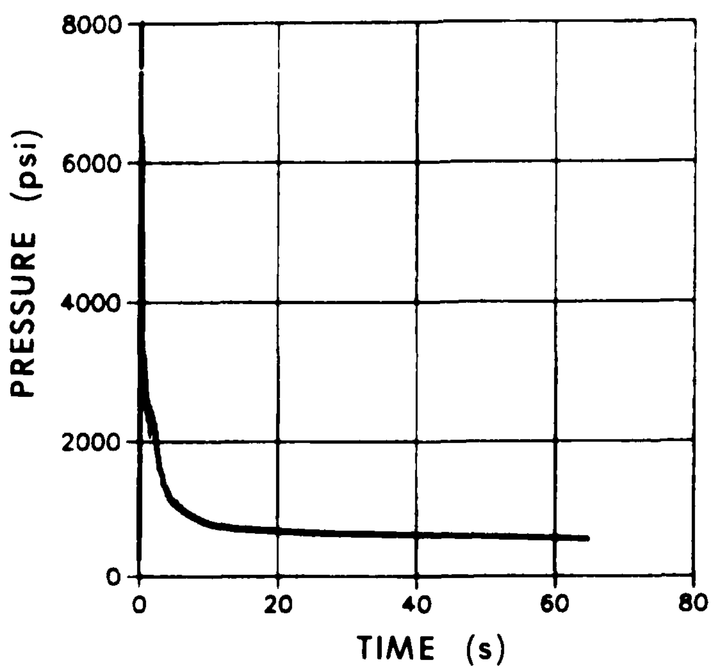

Figure 8. Calculated Pressure History

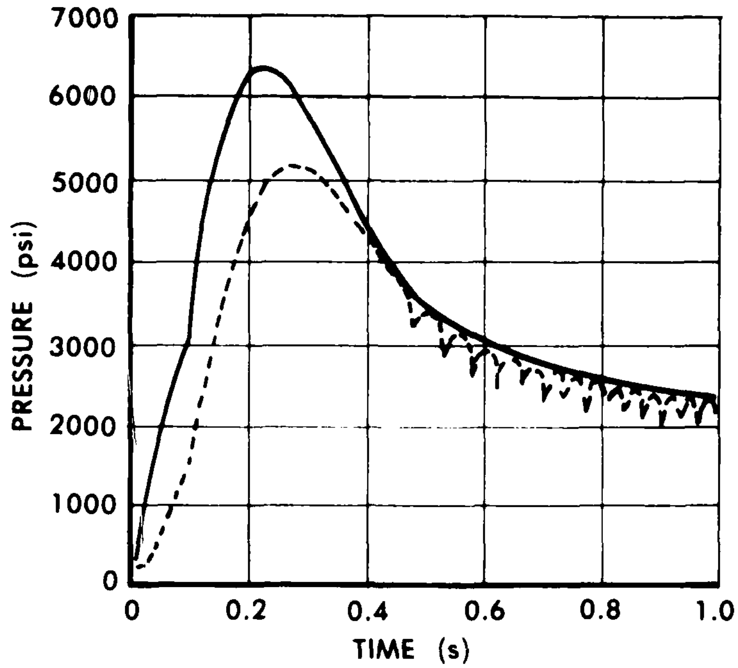

Figure 5. Predicted Pressures at Early Time

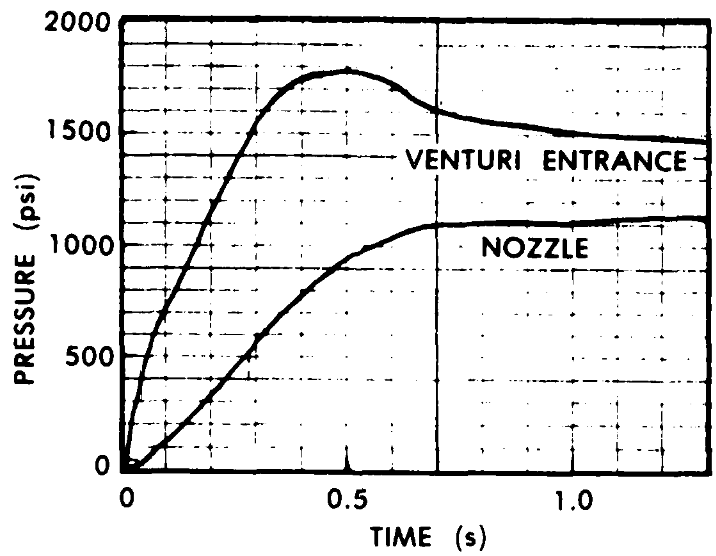

Figure 6. Test Pressures at Early Time

Figure 7 shows a typical cold-temperature test history. The results also miss the measured difference between venturi entrance and nozzle pressures. A consistent difference gap of at least 0.7 MPa appears in the test data but not

momentum

$$P_2 + \omega_2 u_2 = P_3 + \omega_3 u_3 \tag{32}$$

energy

$$\omega_2 (h_2 + u_2^2/2) = \omega_3 (h_3 + u_3^2/2) + \frac{2L_v}{r_w} q_{wv} \quad .$$

The jump equations for flow through the area change, 3→4, are similar to the above set. The system is completed by the addition of Eq. (19) written along the left-running characteristic line which intersects point 4; this provides the communication link to the flow in the downstream tube and nozzle. The total system of equations was hand reduced to four equations in four unknowns and solved with the stiff-equation root finder.

The equations governing the unchoked (subsonic) operation of this element are similar to the above, without the complication of the normal shock wave.

The crucial decision whether the venturi element is choked or unchoked is based on the solution to the complete equation system. If, during the choked solution, the upstream shock Mach number is driven below unity, the solution procedure switches to the unchoked equations and retries the solution. If, during the unchoked solution, the effective choked area [implicit in Eq. (31)] falls below the geometric throat area, a switch is made to the choked equations.

Convective heat transfer to the steel valve and tubing assumes fully-developed turbulent pipe flow; the heat transfer coefficient [for Eq. (5)] is given by

$$h_c = 0.025 \frac{k}{D} Pr^{0.4} (Re_D)^{0.8} \quad .$$

The massive steel valve is assumed to be an infinite sink, but the outer surface of the tubing is allowed to radiate as a black body to the cold ambient temperature. A compromise solution in the combustion chamber assumes heat loss to infinitely thick steel walls at a rate ten times that for stagnant flow, i.e., Nusselt number = 20.

VI. RESULTS

A. Lumped-Parameter Model

For the nominal design and conditions (see Table 1) the predicted early pressure is shown in Figure 5. Peak pressure far exceeds the measured peak as seen in Figure 6, although the time of the peak nearly coincides with test data. Time to peak depends weakly on pressure because it depends on burning rate of the pellet which itself has a low pressure dependence.

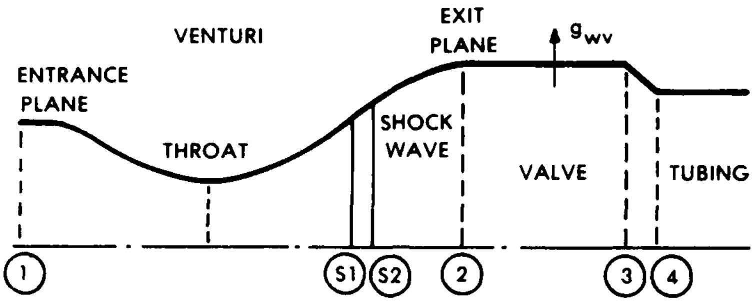

Figure 4. Schematic and Notation for Venturi-Valve Element

For the case when the venturi is choked, the solution for the entrance flow (1) is uncoupled from the flow downstream of the throat and can be found in the manner described in paragraph C above for the choked nozzle. In the region downstream of the throat, Eq. (28) becomes a relationship between the area location of the normal shock wave, A_{sw}, and the upstream Mach number, M_{S1}, ie.,

$$A_{sw} = \{A_{tv}/G_f \; M_{S1}\} \; [1 + \frac{\gamma - 1}{2} M_{S1}{}^2]^{\frac{\gamma + 1}{2(\gamma - 1)}} \quad . \tag{30}$$

Further algebraic manipulation provides a transcendental expression between the downstream shock Mach number, M_{S2}, and the exit plane Mach number, M_2

$$A_{sw} \; M_{S2} \; F_{M2}{}^{\frac{\gamma + 1}{2(\gamma - 1)}} - A_2 \; M_2 \; F_{MS2}{}^{\frac{\gamma + 1}{2(\gamma - 1)}} = 0 \tag{31}$$

where $F_{M2} \equiv 1 + \frac{\gamma - 1}{2} M_2{}^2$

$$F_{MS2} \equiv 1 + \frac{\gamma - 1}{2} M_{S2}{}^2 \quad .$$

When the Mach numbers are determined, total pressure loss across the shock wave and the new stagnation conditions are simple to compute. The equations describing flow in the valve, accounting for heat loss to the boundary, are given by

<u>mass</u>

$$\omega_2 = \omega_3$$

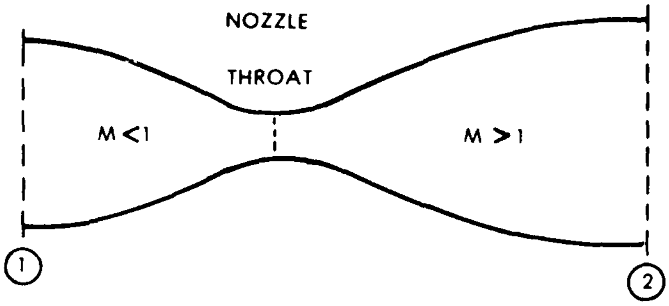

Figure 3. Schematic and Notation for Choked Nozzle Element

Isentropic flow provides a unique relationship between area ratio and Mach number, viz.

$$\frac{\text{choked area}}{\text{local area}} = \frac{A^*}{A} = G_f \, M \left\{1 + \frac{\gamma - 1}{2} M^2\right\}^{-\frac{\gamma + 1}{2(\gamma - 1)}} \tag{28}$$

$$\text{where } G_f \equiv \left(\frac{\gamma + 1}{2}\right)^{\frac{\gamma + 1}{2(\gamma - 1)}} \quad .$$

Given the area ratio, Eq. (28) is a transcendental expression for M which changes only when gas composition, γ, changes. At the entrance plane, Eq. (28) determines M_1 which also must satisfy

$$\rho_1 u_1^2 - \gamma P_1 M_1^2 = 0 \quad . \tag{29}$$

This relationship, along with Eqs. (18) and (20) evaluated at the entrance plane, uniquely determine the flow properties at 1. It is important to note that this choked nozzle solution responds (instantaneously) to any changes in entrance-plane properties; it does not enforce a time-independent value of choked mass flow rate.

D. Venturi-Valve Element

Construction of this element follows that of the nozzle but is more complex. It consists of a converging and diverging section which is attached to a constant-area valve terminated by an area change to match the diameter of the tubing section leading to the nozzle (see Figure 4). Depending upon the overall static pressure difference, this element can operate unchoked with subsonic flow throughout, or choked with a normal shock wave standing somewhere in the divergent section. In both cases, the flow field is assumed quasi-steady and isentropic, with provisions for the shock wave (if present) and wall heat loss in the valve.

q_{wc} = heat loss through wall area A_{wc} of combustion chamber

Obviously, chamber pressure, P_c, follows from the equation of state, $P=P(\rho,e)$.

The separator chamber contains no combustible material and hence has constant volume, V_{sc}. The remaining equations are:

mass

$$\frac{d\rho_{sc}}{dt} = \frac{1}{V_{sc}} [\omega_{C1} A_{C1} - \omega_{T2} A_{T2}] \tag{24}$$

energy

$$\frac{d(\rho_{sc} e_{sc})}{dt} = \frac{1}{V_{sc}} [\omega_{C1} A_{C1} (h_{C1} + u_{C1}^2/2) - \omega_{T2} A_{T2} (h_{T2} + u_{T2}^2/2) - q_{wsc} A_{wsc}] \quad . \tag{25}$$

For low speed flow, the mass flux ω_{C1} between chambers can be written as [e.g., see Ref. 2, p. 95]

$$\omega_{C1} = C_{D_{C1}} P_c \left[\frac{\gamma\beta}{RT_c} \right]^{1/2} (1 + \frac{\gamma - 1}{4} \beta) \tag{26}$$

where β is the solution to

$$\beta (1 + \beta/4) = \frac{2}{\gamma} \left(\frac{P_c - P_{sc}}{P_c}\right) \tag{27}$$

with a similar construction for ω_{T2}. The influence of the pipe/tubing flow is communicated by the compatibility condition [Eq. (19)] along the left-running line reaching the plane T2. With this addition, the dual-chamber flow is uniquely determined. The resulting equation system, however, is quite stiff; a special stiff-equation root finder is required for solution.

C. Choked Nozzle Element

This special solution element (see Figure 3) assumes that the nozzle remains choked, the flow field is quasi-steady, and isentropic. The implication of quasi-steady is that the ratio of nozzle length to local sound speed is much less than the time required for a change in the system flow field. This should be a good assumption here.

---

[2] A.H. Shapiro, Compressible Fluid Flow, Vol. I, Ronald Press, 1953.

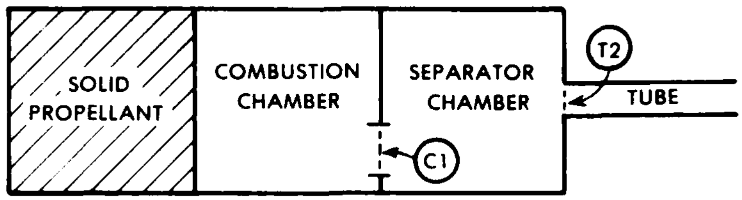

Figure 2. Schematic and Notation for Combustion Chamber Model

Low speed flow ($M^4 \ll 1$) is a reasonable assumption, as are spatially uniform pressure and zero mass-average velocity in each chamber. Real-world flow losses in transfering mass between chambers and into the tubing entrance are modeled with "orifice-loss" coefficients.

For the combustion chamber:

<u>volume change</u>

$$\frac{dV_c}{dt} = Z_{v_I} + Z_{v_{II}} \tag{21}$$

$$\text{where} \quad Z_{v_I} \equiv A_{S_I} r_I \tag{21a}$$

$$Z_{v_{II}} \equiv (A_{S_{II}} + A_{MG}) r_{II}$$

<u>mass</u>

$$\frac{d(\rho_c V_c)}{dt} = \rho_I Z_{v_I} + \rho_{II} Z_{v_{II}} - \omega_{C1} A_{C1} \tag{22}$$

<u>energy</u>

$$\frac{d(\rho_c V_c e_c)}{dt} = \rho_I Z_{v_I} h_I^o + \rho_{II} Z_{v_{II}} h_{II}^o \tag{23}$$

$$- \omega_{C1} A_{C1} (h_{C1} + u_{C1}^2/2) - q_{wc} A_{wc}$$

where ω_{C1} = mass flux through orifice area A_{C1}

h_I^o, h_{II}^o = flame enthalpies of the two propellants

TABLE 1. Nominal Data

Propellants		Ignition Pellet (AP)	Main Grain and Booster Pellet
Density	g/cm^3	1.688	1.439
Specific Heat Ratio		1.184	1.28
Molecular Weight		25.6	18.35
Flame Temperature	K	2857.	1306.
Temperature Sensitivity	1/F	.0014	.0013
Burning Rate (for - 25 F)	cm/s		
Function	P in MPa	$.4422P^{0.38}$	$.04579\ P^{0.71}$ for $P < 3.71MPa$ $.06375\ P^{0.46}$ for $P > 3.71MPa$
Rate at 6.9MPa	cm/s	.92	.155

System					
Chamber Volume	cm^3	9.10	Main Grain Volume	cm^3	6.25
Nozzle Area	cm^2	.00245	Venturi Area	cm^2	.0030
Tube Density	g/cm^3	7.76	Phenolic Density	g/cm^3	1.85
Tube Specific Heat	cal/g/C	.11	Phenolic Specific Heat	cal/g/C	.025
Tube Conductivity	cal/cm/s/C	.001	Phenolic Conductivity	cal/cm/s/C	.0001
Tube Diameter	cm	.457	Ambient Temperature	F	-25.0

momentum

$$\omega_t + (\omega u + P)_z = 0 \tag{16}$$

energy

$$\mathcal{E}_t + [(\mathcal{E} + P)u]_z + \frac{2}{r_w} q_w = 0 \tag{17}$$

where $\omega \equiv \rho u, \quad \mathcal{E} \equiv \rho(e + u^2/2)$

and $P=P(\rho,e)$ is prescribed by the equation of state. The numerical solution is predicted with MacCormack's explicit scheme. Coupling between this unsteady solution and the special flow field elements discussed below is accomplished with method-of-characteristics compatibility conditions along characteristic directions, all of which follow from the above equation system written in characteristic form:

$$dP + \rho a \, du = -Q dt \tag{18}$$

$$\text{along } \frac{dz}{dt} = u + a \qquad \text{(right-running characteristic line)}$$

$$dP - \rho a \, du = -Q dt \tag{19}$$

$$\text{along } \frac{dz}{dt} = u - a \qquad \text{(left-running characteristic line)}$$

$$dP - a^2 d\rho = -Q dt \tag{20}$$

$$\text{along } \frac{dz}{dt} = u \qquad \text{(streamline)}$$

where $Q \equiv \left(\frac{1}{\rho} \left.\frac{\partial P}{\partial e}\right|_\rho\right) \frac{2}{r_w} q_w$ and $a^2 \equiv \left.\frac{\partial P}{\partial \rho}\right|_e + \frac{P}{\rho^2} \left.\frac{\partial P}{\partial e}\right|_\rho$.

B. Combustion Chamber and Separator Chamber

The dual chamber problem is modeled as two reservoirs connected by an orifice, C1. The tubing inlet is an outflux boundary, T2, to the separator chamber (see Figure 2).

LIST OF SYMBOLS

a	local sound velocity [see Eq. 20]
A	cross sectional area
A_{MG}	surface area of main propellant grain
A_{t_n}	nozzle throat area
A_{t_v}	venturi throat area
A_S	propellant surface area
c_p, c_v	specific heat at constant pressure, volume
$C_{D_{Cl}}$	orifice loss coefficient [see Eq. 26]
D	diameter of circular cross section ($2r_w$)
e	specific internal energy
$\mathcal{E}$	total energy per unit volume
G_f	defined in Eq. 28
h	specific enthalpy ($e + P/\rho$)
h^o	reference enthalpy (heat of formation)
h_c	convective heat transfer coefficient
k	thermal conductivity
L_v	axial length of valve
M	Mach number
$\mathcal{M}$	molecular weight
P	static pressure
Pr	Prandtl number
q_w	boundary heat flux
r	solid propellant regression rate
r_w	wall radius of circular cross section
Re_D	Reynolds number based on diameter

t	time
T	temperature
u	velocity
v	volume
z	axial distance
Z_v	volume burned, defined in Eqs. 21a & 21b
γ	isentropic index
ρ	density
ω	mass flux (ρu)
$(\ )_t$	partial derivative wrt time
$(\ )_z$	partial derivative wrt distance
$(\ )_c$	pertaining to combustion chamber
$(\ )_{sc}$	pertaining to separator chamber
$(\ )_v$	pertaining to valve
$(\ )_{I,II}$	pertaining to propellant I (Ignition Pellet) II (Main Grain)

DISTRIBUTION LIST

No. Of Copies	Organization
12	Administrator Defense Technical Info Center ATTN: DTIC-DDA Cameron Station Alexandria, VA 22304-6145
1	HQ DA DAMA-ART-M Washington, DC 20310
1	Commander US Army Material Command ATTN: AMCDRA-ST 5001 Eisenhower Avenue Alexandria, VA 22333-0001
1	Commander Armament R&D Center USA AMCCOM ATTN: SMCAR-TDC Dover, NJ 07801
1	Commander Armament R&D Center USA AMCCOM ATTN: SMCAR-TSS Dover, NJ 07801
1	Commander US Army Armament, Munitions and Chemical Command ATTN: SMCAR-ESP-L Rock Island, IL 61299
1	Director Benet Weapons Laboratory Armament R&D Center USA AMCCOM ATTN: SMCAR-LCB-TL Watervliet, NY 12189
1	Commander USA Aviation Research and Development Command ATTN: AMSAV-E 4300 Goodfellow Blvd. St. Louis, MO 63120
1	Director USA Air Mobility Research and Development Laboratory Ames Research Center Moffett Field, CA 94035
4	Commander US Army Research Office ATTN: R. Ghirardelli D. Mann R. Singleton R. Shaw P.O. Box 12211 Research Triangle Park, NC 27709
1	Commander USA Communications - Electronics Command ATTN: AMSEL-ED Fort Monmouth, NJ 07703
1	Commander USA Electronics Research and Development Command Technical Support Activity ATTN: DELSD-L Fort Monmouth, NJ 07703-5301
2	Commander USA AMCCOM, ARDC ATTN: SMCAR-LCA-G, D.S. Downs J.A. Lannon Dover, NJ 07801
1	Commander USA AMCCOM, ARDC ATTN: SMCAR-LC-G, L. Harris Dover, NJ 07801
1	Commander USA AMCCOM, ARDC ATTN: SMCAR-SCA-T, L. Stiefel Dover, NJ 07801

DISTRIBUTION LIST

No. Of Copies	Organization
1	Commander USA Missile Command ATTN: AMSMI-R Redstone Arsenal, AL 35898
1	Commander USA Missile Command ATTN: AMSMI-YDL Redstone Arsenal, AL 35898
2	Commander USA Missile Command ATTN: AMSMI-RK, D.J. Ifshin W. Wharton Redstone Arsenal, AL 35898
1	Commander USA Tank Automotive Command ATTN: AMSTA-TSL Warren, MI 48090
1	Director USA TRADOC Systems Analysis Activity ATTN: ATAA-SL WSMR, NM 88002
1	Commandant US Army Infantry School ATTN: ATSH-CD-CSO-OR Fort Benning, GA 31905
1	Commander USA Army Development and Employment Agency ATTN: MODE-TED-SAB Fort Lewis, WA 98433
1	Office of Naval Research Department of the Navy ATTN: R.S. Miller, Code 432 800 N. Quincy Street Arlington, VA 22217

No. Of Copies	Organization
1	Commander Naval Air Systems Command ATTN: J. Ramnarace, AIR-54111C Washington, DC 20360
2	Commander Naval Ordnance Station ATTN: C. Irish P.L. Stang, Code 515 Indian Head, MD 20640
1	Commander Naval Surface Weapons Center ATTN: J.L. East, Jr., G-23 Dahlgren, VA 22448
2	Commander Naval Surface Weapons Center ATTN: R. Bernecker, R-13 G.B. Wilmot, R-16 Silver Spring, MD 20910
1	Commander Naval Weapons Center ATTN: R.L. Derr, Code 389 China Lake, CA 93555
2	Commander Naval Weapons Center ATTN: Code 3891, T. Boggs K.J. Graham China Lake, CA 93555
5	Commander Naval Research Laboratory ATTN: L. Harvey J. McDonald E. Oran J. Shnur R.J. Doyle, Code 6110 Washington, DC 20375
1	Commanding Officer Naval Underwater Systems Center Weapons Dept. ATTN: R.S. Lazar/Code 36301 Newport, RI 02840

DISTRIBUTION LIST

No. Of Copies	Organization
1	Superintendent Naval Postgraduate School Dept. of Aeronautics ATTN. D.W. Netzer Monterey, CA 93940
6	AFRPL (DRSC) ATTN: R. Geisler D. George B. Goshgarian J. Levine W. Roe D Weaver Edwards AFB, CA 93523
1	Air Force Armament Laboratory ATTN: AFATL/DLODL Eglin AFB, FL 32542-5000
2	AFOSR ATTN: L.H. Caveny J.M. Tishkoff Bolling Air Force Base Washington DC 20332
1	AFWL/SUL Kirtland AFB, NM 87117
1	Director, NASA Langley Research Center Langley Station ATTN: G.B. Northam/MS 168 Hampton, VA 23365
4	Director National Bureau of Standards ATTN J. Hastie M. Jacox T. Kashiwagi H. Semerjian US Department of Commerce Washington, DC 20234
1	Applied Combustion Technology, Inc. ATTN: A.M. Varney P.O. Box 17885 Orlando FL 32860
1	Atlantic Research Corp. ATTN: M.K. King 5390 Cherokee Avenue Alexandria, VA 22314
1	Atlantic Research Corp. ATTN: R.H.W. Waesche 7511 Wellington Road Gainesville VA 22065
1	AVCO Everett Rsch. Lab. Div ATTN: D. Stickler 2385 Revere Beach Parkway Everett. MA 02149
1	Battelle Memorial Institute Tactical Technology Center ATTN: J. Huggins 505 King Avenue Columbus, OH 43201
2	Exxon Research & Eng. Co. ATTN: A. Dean M. Chou P.O. Box 45 Linden NJ 07036
1	Ford Aerospace and Communications Corp. DIVAD Division Div. Hq., Irvine ATTN: D. Williams Main Street & Ford Road Newport Beach, CA 92663
1	General Electric Armament & Electrical Systems ATTN: M.J. Bulman Lakeside Avenue Burlington VT 05401

DISTRIBUTION LIST

No. Of Copies	Organization
1	Aerojet Solid Propulsion Co. ATTN: P. Micheli Sacramento, CA 95813
1	Strategic Systems Program Office ATTN: SP 2731 Washington, DC 20376
1	General Motors Rsch Labs Physics Department ATTN: R. Teets Warren, MI 48090
1	Hercules, Inc. Allegany Ballistics Lab. ATTN: R.R. Miller P.O. Box 210 Cumberland, MD 21501
1	Hercules, Inc. Bacchus Works ATTN: K.P. McCarty P.O. Box 98 Magna, UT 84044
1	Hercules, Inc. AFATL/DLDL ATTN: R.L. Simmons Eglin AFB, FL 32542
1	Honeywell, Inc. Defense Systems Division ATTN: D.E. Broden/ MS MN50-2000 600 2nd Street NE Hopkins, MN 55343
1	IBM Corporation ATTN: A.C. Tam Research Division 5600 Cottle Road San Jose, CA 95193

No. Of Copies	Organization
1	Director Lawrence Livermore Laboratory P.O. Box 808 ATTN: C. Westbrook Livermore, CA 94550
1	Lockheed Missiles & Space Co. ATTN: George Lo 3251 Hanover Street Dept. 52-35/B204/2 Palo Alto, CA 94304
1	Los Alamos National Lab ATTN: B. Nichols T7, MS-B284 P.O. Box 1663 Los Alamos, NM 87544
1	Olin Corporation Smokeless Powder Operations ATTN: R.L. Cook P.O. Box 222 St. Marks, FL 32355
1	Paul Gough Associates, Inc. ATTN: P.S. Gough 1048 South Street Portsmouth, NH 03801
2	Princeton Combustion Research Laboratories, Inc. ATTN: M. Summerfield N.A. Messina 475 US Highway One Monmouth Junction, NJ 08852
1	Hughes Aircraft Company ATTN: T.E. Ward 8433 Fallbrook Avenue Canoga Park, CA 91303
1	Rockwell International Corp. Rocketdyne Division ATTN: J.E. Flanagan/HB02 6633 Canoga Avenue Canoga Park, CA 91304

DISTRIBUTION LIST

No. Of Copies	Organization	No. Of Copies	Organization
3	Sandia National Laboratories Combustion Sciences Dept. ATTN: R. Cattolica D. Stephenson P. Mattern Livermore, CA 94550	1	Thiokol Corporation Huntsville Division ATTN: D.A. Flanagan Huntsville, AL 35807
1	University of Florida Dept. of Chemistry ATTN: J. Winefordner Gainesville, FL 32611	1	Polytechnic Institute of NY ATTN: S. Lederman Route 110 Farmingdale, NY 11735
1	Science Applications, Inc. ATTN: R.B. Edelman 23146 Cumorah Crest Woodland Hills, CA 91364	1	United Technologies ATTN: A.C. Eckbreth East Hartford, CT 06108
1	Science Applications, Inc. ATTN: H.S. Pergament 1100 State Road, Bldg. N Princeton, NJ 08540	2	United Technologies Corp. Chemical Systems Div. ATTN: R.S. Brown R.O. McLaren P.O. Box 358 Sunnyvale, CA 94086
1	University of Texas Dept. of Chemistry ATTN: W. Gardiner Austin, TX 78712	1	Universal Propulsion Company ATTN: H.J. McSpadden Black Canyon Stage 1 Box 1140 Phoenix, AZ 85029
3	SRI International ATTN: G. Smith D. Crosley D. Golden 333 Ravenswood Avenue Menlo Park, CA 94025	1	Veritay Technology, Inc. ATTN: E.B. Fisher P.O. Box 22 Bowmansville, NY 14026
1	Stevens Institute of Tech. Davidson Laboratory ATTN: R. McAlevy, III Castle Point Station Hoboken, NJ 07030	1	Brigham Young University Dept. of Chemical Engineering ATTN: M.W. Beckstead Provo, UT 84601
1	Teledyne McCormack-Selph ATTN: C. Leveritt 3601 Union Road Hollister, CA 95023	1	California Institute of Tech. Jet Propulsion Laboratory ATTN: MS 125/159 4800 Oak Grove Drive Pasadena, CA 91103
1	Thiokol Corporation Elkton Division ATTN: W.N. Brundige P.O. Box 241 Elkton, MD 21921	1	California Institute of Technology ATTN: F.E.C. Culick/ MC 301-46 204 Karman Lab. Pasadena, CA 91125

DISTRIBUTION LIST

No. Of Copies	Organization
1	University of California, Berkeley Mechanical Engineering Dept. ATTN: J. Daily Berkeley, CA 94720
1	University of California Los Alamos National Lab. ATTN: T.D. Butler P.O. Box 1663, Mail Stop B216 Los Alamos, NM 87545
2	University of California, Santa Barbara Quantum Institute ATTN: K. Schofield M. Steinberg Santa Barbara, CA 93106
1	University of Southern California Dept. of Chemistry ATTN: S. Benson Los Angeles, CA 90007
1	Case Western Reserve Univ. Div. of Aerospace Sciences ATTN: J. Tien Cleveland, OH 44135
1	Cornell University Department of Chemistry ATTN: E. Grant Baker Laboratory Ithaca, NY 14853
1	Univ. of Dayton Rsch Inst. ATTN: D. Campbell AFRPL/PAP Stop 24 Edwards AFB, CA 93523
1	Georgia Institute of Technology School of Aerospace Engineering ATTN: E. Price Atlanta, GA 30332
2	Georgia Institute of Technology School of Aerospace Engineering ATTN: W.C. Strahle B.T. Zinn Atlanta, GA 30332
1	Professor Herman Krier University of Illinois Dept. of Mech. Engr./Indust. Engr. 144MEB, 1206 W. Green St. Urbana, IL 61801
1	Johns Hopkins University/APL Chemical Propulsion Information Agency ATTN: T.W. Christian Johns Hopkins Road Laurel, MD 20707
1	University of Minnesota Dept. of Mechanical Engineering ATTN: E. Fletcher Minneapolis, MN 55455
4	Pennsylvania State University Applied Research Laboratory ATTN: G.M. Faeth K.K. Kuo H. Palmer M. Micci University Park, PA 16802

DISTRIBUTION LIST

No. Of Copies	Organization
2	Princeton University Forrestal Campus Library ATTN: K. Brezinsky I. Glassman P.O. Box 710 Princeton, NJ 08540
1	Princeton University MAE Dept. ATTN: F.A. Williams Princeton, NJ 08544
2	Purdue University School of Aeronautics and Astronautics ATTN: R. Glick J.R. Osborn Grissom Hall West Lafayette, IN 47906
2	Purdue University School of Mechanical Engineering ATTN: N.M. Laurendeau S.N.B. Murthy TSPC Chaffee Hall West Lafayette, IN 47906
1	Rensselaer Polytechnic Inst. Dept. of Chemical Engineering ATTN: A. Fontijn Troy, NY 12181
2	Southwest Research Institute ATTN: R.E. White A.B. Wenzel 8500 Culebra Road San Antonio, TX 78228
1	Stanford University Dept. of Mechanical Engineering ATTN: R. Hanson Stanford, CA 94305
1	University of Utah Dept. of Chemical Engineering ATTN: G. Flandro Salt Lake City, UT 84112
1	Virginia Polytechnic Institute and State University ATTN: J.A. Schetz Blacksburg, VA 24061
2	Commander USA AMCCOM, ARDC ATTN: W. Painter J.H. Wander Dover, NJ 07801
1	Commander USA AMCCOM, ARDC ATTN: SMCAR-LC J.H. Grundler Dover, NJ 07801
1	California Institute of Technology Jet Propulsion Laboratory ATTN: L. Strand 4800 Oak Grove Dr Pasadena, CA 91103
2	Martin Marietta Corp. ATTN: M. Kosar R. Classen MP246 P.O. Box 5837 Orlando, FL 32805
2	Talley Defense Systems ATTN: J. Pietz A. Nebgen P.O. Box 849 Mesa, AZ 85201
1	Avco Systems Division ATTN: V. Suozzo 201 Lowell Street Wilmington, MA 01887

DISTRIBUTION LIST

No. Of Copies	Organization
2	Air Research Mfg Co ATTN: C. Stancliffe E. Nickel 2525 W 190 Street Torrance, CA 90509
2	Olin Corporation ATTN: L. Markowitz I. Mishra Drawer G Marion, IL 62959
1	Commander USA Missile Command Pershing Project Manager ATTN: C. Tidwell Redstone Arsenal, AL 35898

Aberdeen Proving Ground

Dir, USAMSAA
ATTN: AMXSY-D
AMXSY-MP, H. Cohen
Cdr, USATECOM
ATTN: AMSTE-TO-F
Cdr, CRDC, AMCCOM
ATTN: SMCCR-RSP-A
SMCCR-MU
SMCCR-SPS-IL

USER EVALUATION SHEET/CHANGE OF ADDRESS

This Laboratory undertakes a continuing effort to improve the quality of the reports it publishes. Your comments/answers to the items/questions below will aid us in our efforts.

1. BRL Report Number____________________ Date of Report__________

2. Date Report Received____________________

3. Does this report satisfy a need? (Comment on purpose, related project, or other area of interest for which the report will be used.)__________

4. How specifically, is the report being used? (Information source, design data, procedure, source of ideas, etc.)__________

5. Has the information in this report led to any quantitative savings as far as man-hours or dollars saved, operating costs avoided or efficiencies achieved, etc? If so, please elaborate.__________

6. General Comments. What do you think should be changed to improve future reports? (Indicate changes to organization, technical content, format, etc.)

CURRENT ADDRESS

Name

Organization

Address

City, State, Zip

7. If indicating a Change of Address or Address Correction, please provide the New or Correct Address in Block 6 above and the Old or Incorrect address below.

OLD ADDRESS

Name

Organization

Address

City, State, Zip

(Remove this sheet along the perforation, fold as indicated, staple or tape closed, and mail.)

— — — — — — — — — FOLD HERE — — — — — — — — — — —

irector
S Army Ballistic Research Laboratory
TTN: AMXBR-OD-ST
berdeen Proving Ground, MD 21005-5066

NO POSTAGE
NECESSARY
IF MAILED
IN THE
UNITED STATES

OFFICIAL BUSINESS
ENALTY FOR PRIVATE USE. $300

BUSINESS REPLY MAIL
FIRST CLASS PERMIT NO 12062 WASHINGTON, DC

POSTAGE WILL BE PAID BY DEPARTMENT OF THE ARMY

Director
US Army Ballistic Research Laboratory
ATTN: AMXBR-OD-ST
Aberdeen Proving Ground, MD 21005-9989

— — — — — — — — — FOLD HERE — — — — — — — — — — —

END

FILMED

8-85

DTIC